International Journal of Hydrogen Energy 202 (2026) 153039

Contents lists available at ScienceDirect

International Journal of Hydrogen Energy

journal homepage: www.elsevier.com/locate/he

Upgrading LOHC-based hydrogen through electrochemical hydrogen compression for fuel cell applications

M. Blasius [a], S. Pappler [a], T. Mader [a], S. Mrusek [a], T. Rüde [a], M. Geißelbrecht [a,*], P. Wasserscheid [a,b,c]

[a] Forschungszentrum Jülich GmbH, Helmholtz-Institute Erlangen-Nürnberg for Renewable Energies (IET 2), Cauerstraße 1, D-91058, Erlangen, Germany
[b] Lehrstuhl für Chemische Reaktionstechnik, Friedrich-Alexander-Universität Erlangen-Nürnberg, Egerlandstraße 3, D-91058, Erlangen, Germany
[c] Forschungszentrum Jülich GmbH, Institute for a Sustainable Hydrogen Economy, Marie-Curie-Str. 5, 52428, Jülich, Germany

ARTICLE INFO

Keywords:
Hydrogen purification
Liquid organic hydrogen carriers (LOHC)
Electrochemical hydrogen compressor (EHC)
Electrooxidation

ABSTRACT

This study focuses on the continuous and efficient supply of purified and compressed hydrogen from Liquid Organic Hydrogen Carrier (LOHC) systems by employing an electrochemical hydrogen compressor (EHC). In detail, we coupled the continuous dehydrogenation of perhydro benzyltoluene operating at a hydrogen release rate of 0.39 $L_n\ min^{-1}$ with an EHC with one single cell and an active membrane area of 250 cm^2. Nafion 212, 115, and 117 membranes with catalyst loadings of 0.3 $mg_{Pt}\ cm^{-2}$ were evaluated at 35–65 °C cell temperature and with current densities ranging from 0.1 to 0.8 A cm^{-2}. For these broad operating conditions, we measured cell voltages, current efficiencies and calculated Nernst voltages to determine the specific energy consumption. The Nafion 212 membrane exhibited the lowest specific energy consumption at 1.65–4.15 kWh $kg^{-1}_{hydrogen}$ for compression from 1 to 20 bar_a and 2.84–4.97 kWh $kg^{-1}_{hydrogen}$ for 1 to 70 bar_a. Furthermore, regeneration strategies to counter poisoning of the platinum anode catalyst by traces of CO were developed. Discontinuous electrooxidation (d-EO) proved favourable, offering fast regeneration at minimal hydrogen loss. The d-EO step was implemented by purging with inert gas for 60 s and by holding the cell voltage at 0.8 V. Using d-EO, we demonstrated 8 h of stable operation, including 19 regeneration cycles with a typical LOHC-based hydrogen quality containing 41.3 ppm of CO and 2.7 ppm of semi volatile compounds (SVOCs). The combination of LOHC dehydrogenation and EHC technology proved to reliably produce hydrogen fulfilling the requirements of the ISO norm 14687-2 standards on wet basis. Our findings thus demonstrate the combination of hydrogen provision, purification and compression that may prove highly attractive for operating future hydrogen filling stations.

1. Introduction

The roll out of hydrogen filling stations (HFSs) for fuel-cell vehicles (FCVs) marks a significant step towards realizing sustainability in the transport sector. In 2022, a pioneering hydrogen filling station was inaugurated by Hydrogenious LOHC Technologies in Erlangen, Germany [1]. The station is supplied with hydrogen in LOHC-bound form, i.e. chemically bound hydrogen is stored in the form of the hydrogen-rich LOHC compound perhydro benzyltoluene in conventional fuel tanks at the station. On demand, a catalytic dehydrogenation reaction releases hydrogen that is purified at the station by a pressure-swing adsorption unit prior to mechanical compression.

The removal of carbon monoxide from LOHC-based hydrogen is a key challenge to meet the purity requirements for fuel cell vehicles. The removal of carbon monoxide is currently not possible using pressure swing adsorption (PSA), the established process for purifying LOHC-based hydrogen. Moreover, mechanical compression is highly energy intensive and requires considerable maintenance [2,3]. Electrochemical hydrogen compression (EHC) offers a promising alternative, combining efficient purification and compression in a single process unit [2,4–6]. Bouwman reported that compressing hydrogen from 10 to 400 bar_a using an EHC-apparatus requires only 3.3 $kWh_{el}\ kg^{-1}_{hydrogen}$ compared to 6.6 $kWh_{el}\ kg^{-1}_{hydrogen}$ for mechanical compression [3]. For established system employing PSA purification, Zilm et al. reported a regeneration heat demand of about 0.28 % of the hydrogen LHV, which corresponds to roughly 0.1 $kWh_{el}\ kg^{-1}_{hydrogen}$ when expressed as electrical energy [7]. In contrast, electrochemical hydrogen compressors perform purification and compression within a single unit, meaning that the reported 3.3

* Corresponding author.
E-mail address: m.geisselbrecht@fz-juelich.de (M. Geißelbrecht).

https://doi.org/10.1016/j.ijhydene.2025.153039
Received 24 July 2025; Received in revised form 8 December 2025; Accepted 12 December 2025
Available online 17 December 2025

kWh_{el} $kg_{\text{-1hydrogen}}$ already includes purification.

The main challenges of EHC technology lie in hydrogen back-diffusion and membrane deformation due to the pressure differences between in- and outlet [8]. However, commercial manufacturers such as HyET have already developed containerized EHC solutions for HFSs, offering capacities of up to 120 $kg_{hydrogen}$/day with inlet pressures of around 3 bar_a and outlet pressures reaching up to 950 bar_a [9].

Fig. 1 illustrates the concept of a hydrogen filling station operating on the combination of LOHC dehydrogenation and EHC. Hydrogen can be produced sustainably from renewable energy through electrolysis, where water is split into hydrogen and oxygen. By binding hydrogen to an LOHC molecule renewable energy can be stored as well as transported safely and effectively utilizing existing infrastructure for fuels [10–13]. Several LOHC systems have been proposed for hydrogen storage, including methylcyclohexane/toluene (MCH/TOL), perhydro dibenzyltoluene/dibenzyltoluene (H18-/H0-DBT) and perhydro benzyltoluene/benzyltoluene (H12-/H0-BT). Among these, the H12-/H0-BT pair offers notable advantages due to its lower viscosity compared to H18-/H0-DBT system, ensuring better pumpability at low temperatures, as well as its lower vapor pressure and higher volumetric storage density related to the MCH/TOL system. The lower vapor pressure simplifies the separation of the released hydrogen from the LOHC molecule [10]. Moreover, this LOHC system is already well developed, with pilot plants demonstrating continuous hydrogen release capacities of up to 70 $t_{hydrogen}$ per year [1]. The handling of the H12/H0-BT by-passes all challenges associated with high-pressure or cryogenic hydrogen handling. At the LOHC-based hydrogen filling station, the endothermic dehydrogenation of H12-BT is initiated releasing the stored hydrogen. The thereby recovered hydrogen-lean H0-BT can then be returned to the hydrogen production site for re-hydrogenation thus closing the LOHC storage cycle [14].

The H12-BT dehydrogenation process produces hydrogen typically at $\leq$5 bar_a and a purity grade equivalent to 3.0 or 99.9 % [7,15]. The quality of the produced hydrogen which is characterized by its pressure level and purity is insufficient for direct use in FCVs. Regarding the pressure level it is common to store hydrogen at filling stations in buffer pressure vessels with maximum pressures of 50–100 bar_a (depending on the respective design) prior to further compression to the required pressure level for the filling of FCVs [16,17]. Regarding the purity of hydrogen, the ISO 14687-2 defines specific concentration limits for FCVs, which must be met, as shown in Table 1 [18].

Table 1 shows also the impurities in the hydrogen released from H12-BT dehydrogenation measured by Zilm et al. To meet the ISO specification, carbon dioxide (CO_2) and methane (CH_4) pose no problems while carbon monoxide (CO), water (H_2O) and total hydrocarbon (THC) levels exceed the limits for FCVs. Zilm et al. detected a wide range of CO concentrations with increasing H12-BT dehydrogenation temperatures and pressures resulting in lower CO concentrations. They attributed this correlation to the methanation of CO at the dehydrogenation catalyst with platinum as active species. At the highest temperature and pressure, Zilm et al. achieved a CO concentration of 0.1 ppm, which is below the limit specified in the ISO norm for FCVs. At all other operating points, however, the CO concentration exceeds the limit value of 0.2 ppm and further purification is needed [7].

The THC content in the released hydrogen from LOHC systems can be classified into volatile organic compounds (VOC) and semi-volatile organic compounds (SVOC). As VOC especially benzene (C6), toluene (C7) and their hydrogenated counterparts are reported as impurities. Zilm et al. attributed the VOC contamination to the hydrogenolysis of SVOC species. Hydrogenolysis is favoured by high hydrogen partial pressures and elevated temperatures. SVOCs are H12-, H6- and H0-benzyltoluene (C14) isomers and their concentration in the hydrogen product stream depends on the condenser temperature after the dehydrogenation reactor. According to Zilm et al., the SVOC concentration can be estimated with reasonable accuracy based on vapor pressure correlations derived from measurements with a transpiration method developed by Verevkin et al. [19] The THC levels exceed the limit specified in the ISO norm by a factor of 1000. Thus, special measures are needed to separate hydrocarbon impurities from the product hydrogen gas for meeting the 2 ppm limit [7,18].

Mrusek et al. [5] demonstrated for the first time the simultaneous compression and purification of LOHC-based hydrogen utilizing electrochemical hydrogen compression (EHC) technologies. The data given in Table 1 were obtained from H18-DBT dehydrogenation in semi-batch mode (which is not steady-state due to the decreasing H18-DBT concentration over time) by averaging impurities quantified over a 3 h dehydrogenation period. A three-stage purification was used by these authors downstream of the H18-DBT dehydrogenation to purify the raw hydrogen coming from the hot hydrogen release reactor: i) A condenser was operated at 5 °C; ii) subsequently, an activated carbon filter was used to effectively remove remaining VOCs and SVOCs; iii) subsequently, the resulting pre-purified hydrogen was fed to an EHC. The resulting purity of the hydrogen leaving the EHC met the ISO norm 14687-2 specification on a wet basis. Note, that the hydrogen leaving an EHC unit is saturated with water due to the need to humidify the Nafion membrane in the EHC to ensure sufficient proton conductivity [5].

Mrusek et al. [5] periodically purged the anode compartment with hydrogen every 3–5 min to remove accumulated impurities. Among the

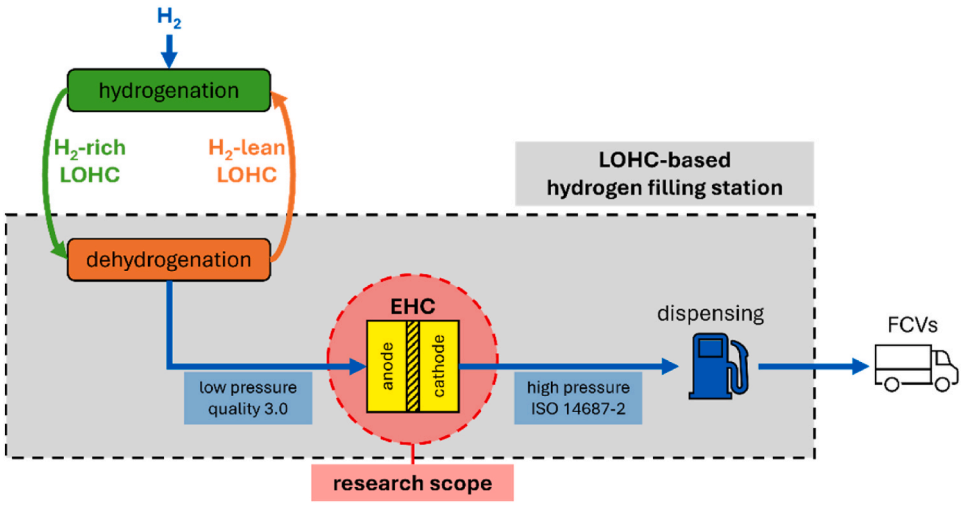

Fig. 1. Concept of a LOHC-based hydrogen filling station with an electrochemical hydrogen compressor (EHC) for simultaneous purification and pressurization of the hydrogen from the LOHC dehydrogenation process.

Table 1
Hydrogen purity specification for polymer electrolyte membrane (PEM) fuel cell vehicles (FCVs) according to ISO 14687-2 [18] compared to the purity of raw hydrogen from the perhydro-benzyltoluene (H12-BT) [7] and perhydro-dibenzyl-toluene (H18-DBT) [5] dehydrogenation as well as hydrogen purity after EHC operation as measured by Mrusek et al. [5] In addition, the reaction conditions in the respective dehydrogenation reactors and the condenser temperatures in the dehydrogenation systems are given.

Impurities/ppm	Required H_2 purity for FCVs (ISO 14687-2) [18]	Raw H_2 purity from H12-BT dehydrogenation (Zilm et al.) [7]	Raw H_2 purity from H18-BT dehydrogenation (Mrusek et al.) [5]	H_2 purity after EHC purification (Mrusek et al.) [5]
CO	0.2	0.1–13.1	1.5	0.0
CO_2	2	0.3–1.7	6.9	0.0
CH_4	100	18.2–36.7	120.5	0.1
H_2O	5	<LOQ[a] – 220.1	not specified	wet
THC (C1-equivalent)	2	1044.0–3433.4	609.7	<2[b]
Dehydrogenation temperature	–	290–330 °C	240 °C	–
Dehydrogenation pressure	–	3–5 bar_a	1.0 bar_a	–
Condenser temperature	–	30 °C	5 °C	–

[a] Limit of quantification.
[b] Mrusek et al. detected 12.9 ppm THC in hydrogen 5.0, leading to the conclusion that THC level was below 2 ppm threshold specified by ISO 14687-2.

detected impurities were traces resulting from air leakage into the system as the dehydrogenation was conducted at atmospheric or sub-atmospheric pressures down to 0.5 bar_a. This work impressively indicated that all impurities present in the hydrogen after condensation and active carbon filtration pose no problem for the stable operation of an EHC. The observed system stability may surprise at the first glance as it is known from literature, that the traces of CO present in the product gas should act as catalyst poison for the platinum catalyst in the EHC [20,21]. It is assumed that the traces from air leakage (see above) lead to an oxidation of CO to CO_2, which then desorbs from the Pt surface in an air bleeding-type regeneration mechanism [22,23].

While hydrogen purging alone is known to not remove adsorbed CO to regenerate an EHC, air bleeding and electrooxidation strategies have been outlined in the literature as suitable regeneration measures [22–26]. For the air bleeding, air is purposedly used to oxidize the CO adsorbed on platinum (see Equation (1)) [27]. The resulting CO_2 rapidly desorbs from the catalyst and passes into the gas phase liberating an active catalyst site again. A more detailed description regarding the mechanism can be found in the ESI in section 1.

$$CO - s + \frac{1}{2}O_2 \rightarrow CO_2 + s_0 \quad (1)$$

Nordio et al. [25] explored the separation of hydrogen with an EHC from a H_2/CO_2 mixture containing CO. They demonstrated that a single bleeding with air for 5 s through the anode compartment was sufficient to regenerate the cell after CO poisoning. For this strategy the EHC operation was interrupted resulting in a discontinuous air bleed regeneration process. Jackson et al. [24] investigated, in contrast, a continuous air bleeding regeneration. In their study, they introduced hydrogen gas containing 20 ppm CO into their EHC setup containing a Pt-catalyst in the membrane electrode assembly (MEA). While they observed a continuously decreasing current at a potentiostatic hold of 100–200 mV, the continuous introduction of 1.2 $\%_{vol}$ oxygen into the EHCs feed could maintain a constant current for 15 min. However, the continuous air bleeding resulted in a current loss of 20–60 % compared to pure hydrogen operation.

Note, that also thermal and chemical membrane degradation needs to be considered with continuous air bleed regeneration. Heat generation due to direct combustion of hydrogen is less relevant because heat generation from the membrane resistance is in the same order of magnitude. According to literature, chemical degradation is more an issue [28]. When oxygen is reduced on the Pt-catalyst at low potentials (<0.2 V) peroxides can be formed. These do not directly cause membrane degradation, but they can form oxygen radicals with impurities in the MEA, such as Cu^{2+} or Fe^{2+} ions, which then lead to membrane degradation.

For the electrooxidation mechanism, potentials of ≥0.57 V versus the standard hydrogen electrode (SHE) are applied (Equation (2)). This potential is the lower limit for the formation of an adsorbed OH group on platinum. The adsorbed OH group is crucial for initiating the oxidation of CO to CO_2 [29]. It should be noted that there is also an upper limit for the applied potential due to irreversible platinum dissolution. Cherevko et al. [30] stated that platinum in a Nafion-based fuel cell gets susceptible to dissolution in the potential range between 0.92 and 1.10 V versus SHE. To avoid platinum dissolution the potential during regeneration should therefore be smaller than 0.92 V. A more detailed description regarding the mechanism can be found in the ESI in section 1.

$$\text{anode } CO - s + H_2O \rightarrow CO_2 + s_0 + 2H^+ + 2e^- \quad (2)$$

$$\text{cathode } 2H^+ + 2e^- \rightarrow H_2 \quad (3)$$

$$CO - s + H_2O \rightarrow s_0 + CO_2 + H_2 \quad (4)$$

The electrooxidation mechanism was investigated by Gardner et al., [26] who fed a mixture of 80 $\%_{vol}$ H_2 and 20 $\%_{vol}$ CO_2 containing 1000 ppm CO into their EHC setup. These authors observed an increase in cell voltage, which could be counter-acted by applying a voltage pulse of 0.7 V for 0.5 s in 10-s intervals for 30 s. This process effectively restored the initial voltage levels, demonstrating the feasibility of what will be referred to as continuous electrooxidation regeneration.

The aim of this study is to use an EHC as a single downstream unit operation to efficiently upgrade hydrogen from the H12-BT dehydrogenation to provide sufficiently purified and compressed hydrogen for FCV filling stations with a minimal specific energy consumption. In this context, the energetic evaluation focuses solely on the electrical energy demand of the EHC as the efficiency of the LOHC dehydrogenation strongly depends on the specific heat integration concept applied in the dehydrogenation process [31]. We will evaluate how to select the optimal membrane type and operating conditions based on investment and operating costs. Furthermore, we will describe a comprehensive regeneration strategy for stable operation of the EHC using LOHC-based hydrogen which contains CO concentrations. This is essential for continuous operation of the EHC without permanent performance decay. Ultimately, the hydrogen output quality is evaluated.

2. Experimental

Our experimental setup included a continuous LOHC-dehydrogenation unit (see Fig. 2) and an electrochemical hydrogen compressor (EHC) unit (see Fig. 3).

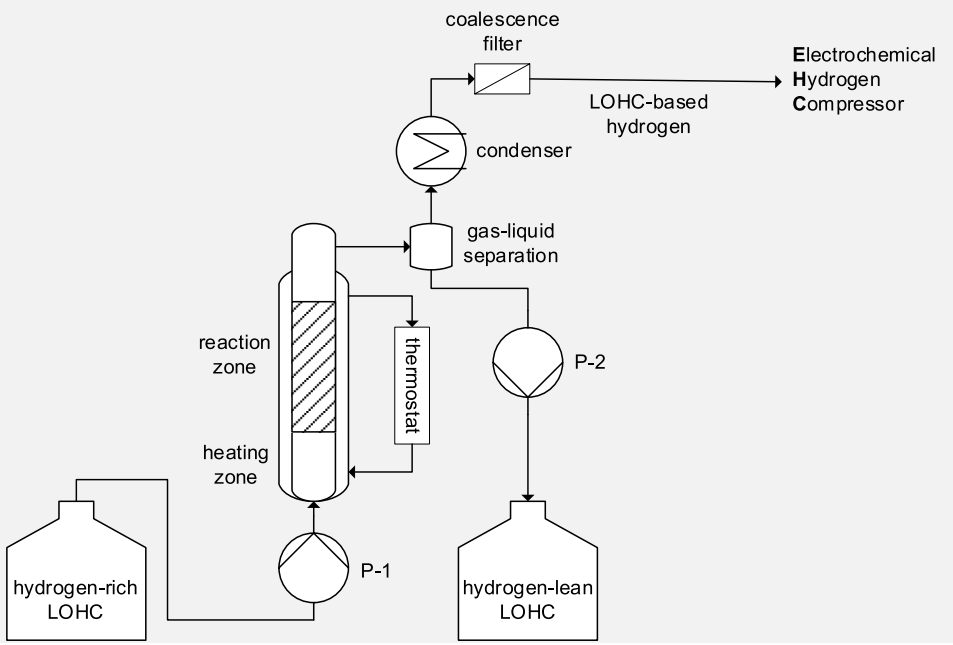

Fig. 2. Simplified flow chart of the LOHC-dehydrogenation unit.

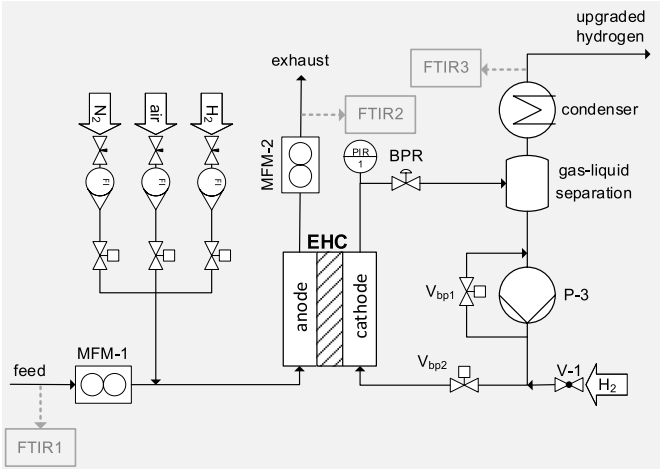

Fig. 3. Simplified flow chart of the electrochemical hydrogen compression unit.

2.1. LOHC-dehydrogenation unit

The main part of the LOHC-dehydrogenation unit was a glass reactor with a double-walled jacket for heating (Fig. 2). Thus, the reactor could only be operated at atmospheric pressure. The jacket was operated with thermal oil, circulated by a thermostat (Huber, Unistat TR401w HT) to maintain the temperature. Hydrogen-rich LOHC, namely perhydro benzyltoluene (H12-BT), was fed into the reactor using a micro-gear pump P-1 (HNP, mzr-2905). A heating zone at the reactor inlet raised the temperature of the feed to thermal oil temperature. The subsequent reaction zone, 20 mm in diameter and 265 mm in length, contained 60 g of Clariant's EleMax-102D catalyst. The catalyst consisted of 0.3 wt.-% platinum on spherical γ-Al_2O_3 particles with a diameter of 2–4 mm. To obtain the temperature in the reaction zone ($T_{reactor}$), values of five equidistant measurement points from a multipoint thermocouple installed in the centre of the catalyst bed were averaged. When the H12-BT contacted the catalyst, it released hydrogen to form hydrogen-lean LOHC (Hx-BT). The hydrogen was pre-purified downstream of the reactor. The Hx-BT was condensed at a temperature of 5 °C and separated in a gas-liquid separator before being transferred to the product tank by another micro-gear pump P-2 (HNP, mzr-2905). Any remaining liquid droplets were removed from the LOHC-based hydrogen using a coalescence filter.

2.2. EHC unit

The EHC unit (Fig. 3) used a single-cell TP250v2 from Tandem Technologies. The active area of the MEA was 250 cm^2, defined by the cell geometry (26.65 cm × 9.75 cm). The anode and cathode flow fields were made of graphite, each containing 61 horizontally aligned channels. Channel dimensions were 0.50 mm × 0.50 mm on the anode and 0.79 mm × 0.79 mm on the cathode side. Silicone gaskets were used for sealing. The cell temperature was controlled between 35 and 65 °C using a thermostat (Huber, Piccolo Ole 280), which circulated distilled water around the anode and cathode flow fields. The cell was assembled with six bolts tightened by round nuts, and sealing was ensured by applying an external compression pressure of approximately 8.3 bar_a, maintained via an electronic pressure control valve (Pressure Control Solutions B.V., PCS-DV-A-10PG-AG). DC power was provided by a LAB/HP415 from ET System (0–500 A, 0–15 V). Galvanostatic holds were carried out with the EHC by setting a current and measuring the resulting voltage at designated points on the anode and cathode flow fields using a voltmeter (Keysight, EDU34450A). Three types of membrane electrode assemblies (MEAs) were used, with Nafion membranes of 50, 125, and 175 µm thickness (N212, N115, N117). Each MEA used carbon cloth W1S1011 with 0.3 mg cm^{-2} of platinum (40 % Pt/C) as a gas diffusion electrode (GDE).

The single-cell EHC had connections for feed inlet and outlet at the anode. Nitrogen, synthetic air, and hydrogen were available via solenoid valves for purging the anode. During the purging process, a fourth solenoid valve directed the feed into the exhaust. The adjustment of the gas flow rates was achieved using float-type flow meters (Voegtlin, Q-Flow 140) located before the solenoid valves.

Three types of feed gases have been studied in this work for operation with the EHC:

- Hydrogen 5.0 from the laboratory gas supply,

- model hydrogen from a gas bottle mimicking typical impurities from the LOHC dehydrogenation, i.e. containing 5 ppm CO, 5 p.m. CO_2, 25 ppm CH_4, 50 ppm benzene, 50 ppm cyclohexane, 100 ppm toluene and 100 ppm methylcyclohexane,
- hydrogen from the LOHC-dehydrogenation unit.

The amount of supplied hydrogen 5.0 and model hydrogen could be adjusted using a mass flow controller (Bronkhorst, F–201CV–5K0-RGD-33-V), while the gas flow from the LOHC-dehydrogenation unit was predetermined by the operating conditions of the dehydrogenation reactor.

The amount of hydrogen processed by the EHC unit was verified using Faraday's law. By quantifying the inlet and outlet hydrogen flow on the anode side by two mass flow meters (MFM-1 up to 1.0 L_n min^{-1} and MFM-2 up to 0.2 L_n min^{-1} both from Voegtlin, red-y smart meter) the mass balance was closed during operation. The values differed by less than 2 % according to Equation (5):

$$(98\ldots102\%)\cdot\dot{m}_{H_2,MFM1} = \dot{m}_{H_2,MFM2} + \frac{I}{2F\cdot M_{H_2}} \tag{5}$$

On the cathode side a backpressure regulator BPR (Pressure Control Solutions B.V., ZF0/1/2 Series Equilibar) and a pressure sensor PIR (alpha-redline, KMP 331) were applied to adjust the pressure between 1 and 3 bar_a. The BPR allows the gas to pass only once the set outlet pressure is reached and remains closed at lower pressures. After the BPR the pressure was approx. atmospheric. The membrane in the EHC was humidified with liquid distilled water, circulated through the gas-liquid separator using a micro-gear pump P-3 (HNP, mzr-2505). This circulation system could be by-passed by opening the solenoid valve V_{bp1} and closing V_{bp2}. The cathode compartment could be purged with hydrogen via a manual valve V-1 and a MFC (Bronkhorst, F–201CV–5K0-RGD-33-V), which was only operated to conduct hydrogen crossover measurements.

The upgraded hydrogen downstream of the EHC passed through the top of the gas-liquid separator and a condenser with cooling coil and jacket from VWR operated at 5 °C. Impurities in the hydrogen were measured using an FTIR (MKS, MultiGas 2031). In addition to analysing the upgraded hydrogen after the condenser, a three-way valve at the anode inlet and outlet allowed the feed stream to be directed to the FTIR for impurity analyses.

2.3. Key performance indicators

Two key performance indicators (KPIs) were used for the energetic analysis based on experimental and calculated values. The first KPI describes the active membrane area A_M in m^2 required to pump 1 $kg_{hydrogen}$ h^{-1}. A_M is calculated according to Equation (6) with i_{set} being the applied current density and η_c being the current efficiency, F being the faraday constant, and M_{H2} being the molar mass of hydrogen.

$$A_M\left[m^2\right] = \frac{2F\cdot M_{H_2}\cdot 1\ kg_{H_2}\ h^{-1}}{i_{set}\cdot\eta_c} \tag{6}$$

A_M is an indicator for the required EHC investment with smaller A_M indicating lower investment cost.

As a second KPI focusing on the operating costs of the EHC unit the specific energy consumption $E_{specific}$ was determined. $E_{specific}$ is calculated according to our previous work [6] according to Equation (7) and its unit is kWh_{el} $kg^{-1}_{H2,pumped}$.

$$E_{specific}\left[\frac{kWh_{el}}{kg_{H_2,pumped}}\right] = \frac{P_{EHC}}{\dot{m}_{H_2,pumped}} = \frac{(U_{Nernst}+U_{cell})}{\eta_c}\cdot\frac{2F}{M_{H_2}} \tag{7}$$

In Equation (7) P_{EHC} represents the consumed electrical power, $\dot{m}_{H_2,pumped}$ the hydrogen transported through the membrane, F the Faraday constant, and M_{H2} the molar weight of hydrogen.

The Nernst voltage U_{Nernst} is calculated using the Nernst Equation. Hereby, it is important to consider the hydrogen partial pressures in the anode and cathode compartments, rather than the system pressure. Therefore, the vapor pressure of water at the cell temperature is subtracted from the system pressure at the anode and cathode to calculate the partial pressure of hydrogen on both sides.

U_{cell} is the voltage required to overcome the cell resistance comprised of membrane and contact resistance. To determine U_{cell}, polarization curves with hydrogen 5.0 from the laboratory gas supply were recorded at pressures of 1 bar_a on both the anode and cathode sides. The temperature was adjusted to the desired cell temperature (35, 50, 65 °C) using a thermostat. For cell humidification, liquid water was circulated on the cathode side. The hydrogen yields during the polarization curve measurements ranged from 90 to 95 % in all experiments. A galvanostatic hold was performed during the measurements. Defined current densities between 0.1 and 0.8 A cm^{-2} were investigated. The voltage at each selected current density was measured using a voltmeter.

$$\eta_c = \frac{\dot{n}_{H_2,pump} - \dot{n}_{H_2,crossover}}{\dot{n}_{H_2,pump}} \tag{8}$$

The current efficiency η_c was obtained using a mathematical model. It is dependent on the molar flow rate of pumped hydrogen $\dot{n}_{H_2,pump}$ and the hydrogen crossover molar flow rate $\dot{n}_{H_2,crossover}$ (see equation (8)).

$$\dot{n}_{H_2,pump} = \frac{i_{set}\cdot A_{M,250}}{2\cdot F} \tag{9}$$

$\dot{n}_{H_2,pump}$ was calculated with the applied current density i_{set} and the active membrane area $A_{M,250}$ using Faraday's law (see equation (9)).

$$\dot{n}_{H_2,crossover} = \varepsilon\cdot\frac{\Delta p\cdot A_{M,250}}{d_{membrane}} \tag{10}$$

$\dot{n}_{H_2,crossover}$ was calculated with the permeability coefficient ε, the pressure difference Δp, the active membrane area $A_{M,250}$ and the membrane thickness $d_{membrane}$ (see equation (10)).

$$\varepsilon = \frac{I_{cross}}{2\cdot F}\cdot\frac{d_{membrane}}{\Delta p\cdot A_{M,250}} \tag{11}$$

The permeability coefficient ε in mol cm cm^{-2} s^{-1} bar^{-1} was obtained in crossover measurements. For the measurements, dry nitrogen was fed to the anode at a rate of 0.2 L_n min^{-1}. On the cathode side, water was circulated using the gear-grid pump P-3, and additionally, 0.2 L_n min^{-1} hydrogen was manually fed via V-1. A voltametric hold at 0.2 V was applied using the DC power supply. The desired cell temperature (35, 50, 65 °C) was set using the thermostat. The pressure was maintained at 1 bar_a on the anode side and varied from 1 to 3 bar_a on the cathode side using the back pressure regulator (BPR). At the applied conditions hydrogen passes back through the membrane from cathode to anode side. The resulting crossover current I_{cross} was measured using a digital multimeter (Keysight, EDU34450A). I_{cross} was converted into permeability coefficients ε for hydrogen by using Faraday's law, where ε depends on the cell temperature but is also normalized to membrane thickness and pressure difference (see equation (11)). Using the mathematical model, the experimentally derived cell voltage and the theoretically calculated Nernst voltage, the specific energy consumption of the EHC can be investigated.

3. Results

3.1. Membrane selection for minimum specific energy consumption

Firstly, an analysis was conducted to identify the membrane with the lowest possible specific energy consumption $E_{specific}$ in EHC operation. It should be noted that the following energetic analysis refers exclusively to the electrical energy demand of the EHC. The thermal energy input for the dehydrogenation of H12-BT is not considered [31]. In this context, the required active membrane area A_M to pump 1 kg of hydrogen per

hour is discussed. This chapter focuses exclusively on the operation of the EHC with hydrogen 5.0.

Polarization curves to determine U_{cell} were recorded at 35 °C, 50 °C, and 65 °C for different membrane thicknesses (N212, N115, and N117) and current densities ranging from 0.1 to 0.8 A cm^{-2}. Fig. 4 shows that with rising cell temperature and decreasing membrane thickness, the membrane resistance drops, leading to a lower cell voltage U_{cell}. However, when current density increases, membrane resistance stays constant, but cell voltage rises due to higher flow based on Ohm's law. The cell voltages measured at 50 °C fall in-between those measured at 35 °C and 65 °C and can be found in the ESI (Tables S1–S6). The observed trends align well with the literature [32].

Stable operation of the EHC was possible for current densities up to 0.8 A cm^{-2} with Nafion 212 and 0.4 A cm^{-2} with Nafion 115 and 117. This behaviour is due to water management within the cell. The membrane is humidified on the cathode side, and water diffuses to the anode. However, this diffusion is opposed by the electroosmotic drag (EOD). Beyond a certain point, EOD disrupts stable humidification, making consistent EHC operation impossible. Thinner membranes facilitate higher current densities compared to thicker ones.

Next, crossover measurements were carried out to determine the hydrogen permeability and its back diffusion from the cathode to the anode. In this way the membranes current efficiencies η_c can be evaluated. The literature values for comparison were taken from Schalenbach et al. [33] These authors worked with N212, N115, and N117 membranes at cathode pressures up to 4.5 bar_a and an anode pressure of 1 bar_a. They determined the permeabilities of dry and humidified Nafion at temperatures of 30 °C, 55 °C, and 80 °C [33]. Hydrogen permeates through Nafion solely via diffusion with the permeability being influenced by the membrane's temperature and humidity [33]. As shown in Fig. 5, all measurements show an exponential increase in permeability with increasing temperature, which is consistent with the results of Schalenbach et al. according to which the gas permeability through a polymer is governed by a thermally activated diffusion described by the Boltzmann distribution [33].

The permeability coefficients in our experimental setup are slightly lower than those measured by Schalenbach et al. for fully humidified Nafion. This suggests that the membranes in our setup are not fully humidified. In our setup during crossover measurements, the anode input stream was dry nitrogen to simulate real operation with dry LOHC-based hydrogen, while Schalenbach used humidified nitrogen [33]. As a result, lower hydrogen crossover and better current efficiencies can be achieved compared to fully humidified Nafion. Note, that humidification is necessary to ensure sufficient conductivity of the Nafion membranes.

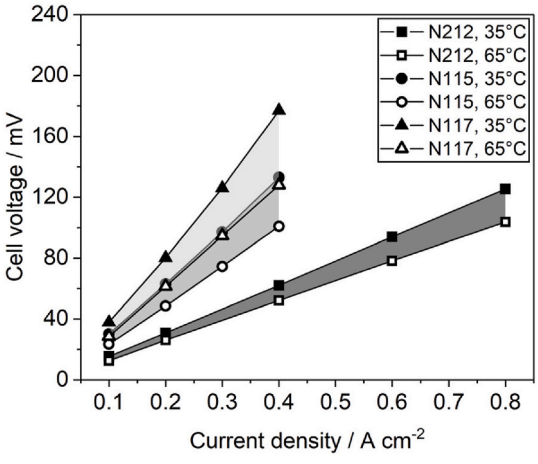

Fig. 4. Polarization curves measured at 35 and 65 °C cell temperature for three different Nafion membranes (N212, N115, N117) with a catalyst loading of 0.3 mg cm^{-2} platinum (40 % Pt/C), carbon cloth W1S1011, active membrane area of 250 cm^2, at yields of 90–95 %; no pressure difference between anode and cathode and dry hydrogen 5.0 as feed. Humidification was realized by circulation of liquid water on the cathode side. Stable operation for Nafion 115 and 117 was not possible above 0.4 A cm^{-2} due to insufficient water management; curves end accordingly.

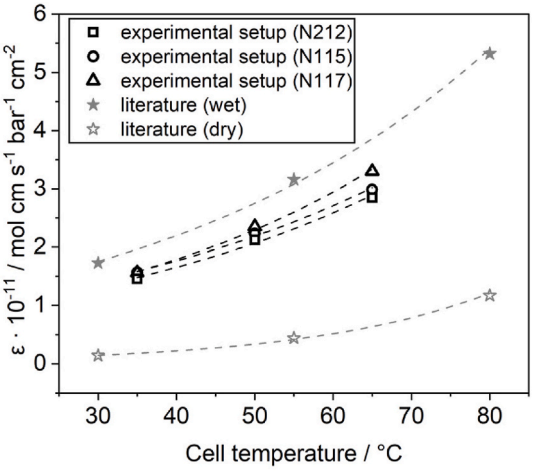

Fig. 5. Permeability coefficient ε of hydrogen through Nafion measured at 35, 50 and 65 °C cell temperature for three different Nafion membranes (N212, N115, N117) with a catalyst loading of 0.3 mg cm^{-2} platinum (40 % Pt/C), carbon cloth W1S1011, and active membrane area of 250 cm^2. Dry nitrogen on the anode and liquid water and hydrogen on the cathode side. Measured ε from our experimental setup are compared to literature values for dry and wet Nafion from Schalenbach et al.. [33].

For the energetic analysis, the measured permeability coefficients were averaged at each cell temperature across all three membrane thicknesses, as summarized in Table 2. The slightly higher permeability coefficients observed for thicker membranes may result from uncertainties in the actual built-in membrane thickness compared to the manufacturer's specified values used in the calculations. Using these permeability coefficients, the hydrogen crossover and corresponding current efficiencies were calculated for all three cell temperatures, all three membrane types and various pressure differences.

With these pre-investigations the specific energy consumption $E_{specific}$ of the EHC unit can be determined considering two scenarios: compression of hydrogen from 1 to 20 bar_a (scenario 1) and from 1 to 70 bar_a (scenario 2). It is assumed that the membrane stability is sufficient for the pressure differences under consideration.

$E_{specific}$ is evaluated using the Nernst Equation while accounting for the vapor pressure of water, the polarization curves, and the current efficiencies calculated from the permeability coefficients for the N212 and N115 membranes. The N117 membrane is left out here since it suffers from 28 to 33 % higher cell voltages due to its increased thickness compared to the N115 at very similar current efficiencies. The comprehensive data sets for $E_{specific}$, including measurements at 50 °C and the N117 membrane, can be found in the ESI (Tables S1–S6).

Fig. 6 depicts $E_{specific}$ for the N115 and N212 membranes evaluated at 35 and 65 °C for scenarios 1 and 2 and current densities ranging between 0.1 and 0.8 A cm^{-2}. With increasing current density, $E_{specific}$ rises, which is attributed to the increasing cell voltage U_{cell} according to Ohm's law.

Table 2
Permeability coefficients ε for hydrogen used for the energetic analysis at three different temperatures averaged for N117, N115, N212 membranes with their uncertainty.

Temperature/°C	ε•10^{-11}/mol cm s^{-1} bar^{-1} cm^{-2}
35	1.53 ± 0.05
50	2.24 ± 0.09
65	3.05 ± 0.19

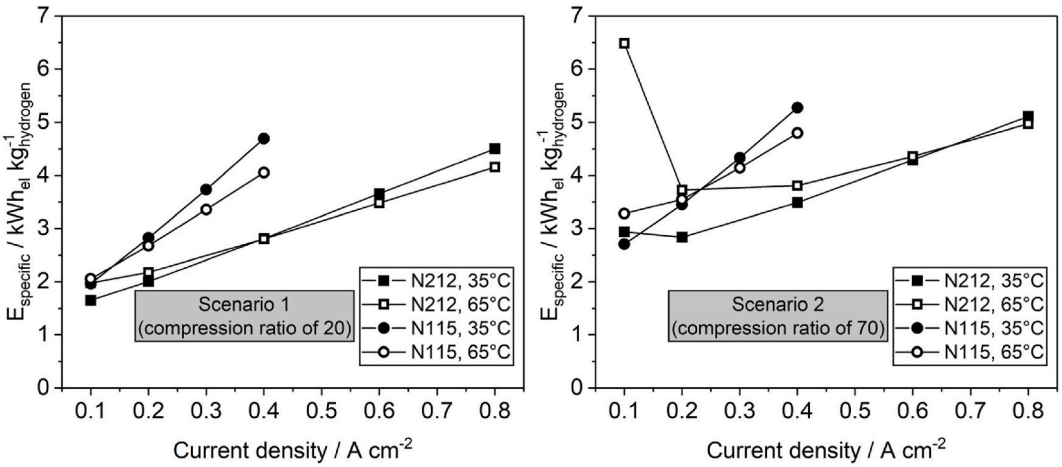

Fig. 6. Specific energy consumption $E_{specific}$ of the EHC per kg of compressed hydrogen for a variation of current densities i_{set} for two different Nafion membranes (N212, N115) each with a catalyst loading of 0.3 mg cm^{-2} platinum (40 % Pt/C). Scenario 1 represents a compression ratio of 20 and scenario 2 represents a compression ratio of 70, respectively.

For Scenario 1 the thinner N212 membrane generally has a lower $E_{specific}$ compared to the N115 membrane. In the compression from 1 to 20 bar_a, the Nafion 212 membrane achieves a $E_{specific}$ between 1.65 and 4.15 kWh_{el} $kg^{-1}_{hydrogen}$.

Comparing $E_{specific}$ at 35 °C and 65 °C for Scenario 1, it is observed that at low current densities $E_{specific}$ is lower for operation at 35 °C while at higher current densities $E_{specific}$ is lower for operation at 65 °C. The point where both curves intersect is observed at approximately 0.4 A cm^{-2} for the N212 membrane and at approximately 0.15 A cm^{-2} for the N115 membrane. This temperature-dependence can be explained by the opposing effects of current efficiency due to hydrogen crossover and cell voltage due to membrane resistance with cell temperature. At low current densities, the $E_{specific}$ is primarily influenced by current efficiency, which is higher at lower temperatures. At high current densities, $E_{specific}$ is mainly affected by the cell voltage, as the current efficiency has minimal impact under these conditions, even at elevated cell temperatures. Thus, a higher cell temperature is advantageous at high current densities due to the lower cell voltages.

For scenario 2, the Nernst voltage is higher and due to the higher pressure difference, the current efficiency is lower compared to Scenario 1 under otherwise identical conditions. Also in Scenario 2, the N212 membrane shows a consistently superior performance compared to the N115 membrane, with a $E_{specific}$ between 2.84 and 4.97 kWh_{el} $kg^{-1}_{hydrogen}$. The intersection point shifts to higher current densities in scenario 2, 0.65 A cm^{-2} for the N212 membrane and 0.25 A cm^{-2} for the N115 membrane. This is due to the stronger influence of hydrogen crossover with the higher pressure difference. The stronger influence of hydrogen crossover also leads to a decrease in $E_{specific}$ for the N212 membrane as the current density increases from 0.1 to 0.2 A cm^{-2} in Scenario 2. The minimal $E_{specific}$ with the N212 membrane for scenario 2 (compression ratio of 70) was found at 35 °C and 0.2 A cm^{-2} with 2.84 kWh_{el} $kg^{-1}_{hydrogen}$.

These two scenarios illustrate that the selection of cell temperature and membrane type depends on the compression ratio, pressure difference and the current density. The compression ratio and pressure difference is given by the operational scenario, while the choice of current density requires consideration of the required active membrane area. This translates to the fact that, in addition to operational costs such as specific energy consumption, investment costs must also be considered, particularly the active membrane area A_M required to pump 1 $kg_{hydrogen}$ h^{-1} A_M.

Table 3 compares active membrane area in m^2 required to pump 1 $kg_{hydrogen}$ h^{-1} A_M in the scenario 2 with the N212 membrane using 35 °C cell temperature and different current densities. As the current density increases, the required active membrane area A_M decreases because more hydrogen is pumped per area. The reduction in A_M is not proportional to the increase in current density due to the minimal influence of current efficiency (see Equation (6)). However, with decreasing A_M investment costs go down.

Table 3
Required active membrane area in m^2 to pump 1 $kg_{hydrogen}$ h^{-1} A_M at 35 °C for scenario 2 with the N212 membrane at different current densities i_{set}.

Current density/A cm^{-2}	0.1	0.2	0.4	0.6	0.8
A_M for 1 $kg_{hydrogen}$ h^{-1}/m^2	40.6	16.1	7.3	4.7	3.5

In summary, the N212 membrane exhibits the lowest $E_{specific}$ for both scenarios evaluated. The optimal cell temperature for minimizing specific energy consumption depends on the chosen current density. Selecting the optimal current density for a given application scenario involves a proper balancing of investment and operating costs.

3.2. EHC regeneration strategies

Impurities in the hydrogen feed to the EHC can lead to reversible poisoning of the platinum catalyst [20,21]. Fig. 7 illustrates the increase of the cell voltage U_{cell} after switching the feed from hydrogen 5.0 to the model hydrogen feed mimicking typical impurities from LOHC-based hydrogen provision. CO was identified as critical for the poisoning of the catalyst since no poisoning was observed with a model hydrogen quality in the absence of CO.

To enable stable EHC operation, the CO-poisoned platinum catalyst was regenerated utilizing both air bleeding or electrooxidation mechanisms. Both can be realized in either a continuous or discontinuous manner (cf. Fig. 9).

In the continuous air bleeding strategy (Fig. 8, A), a small amount of oxygen (<4 $\%_{vol}$ to avoid flammability) is blended into the feed stream of the EHC. The blended oxygen reacts with the CO to form CO_2 which rapidly desorbs and thereby regenerates the platinum centres. It is noteworthy that this regeneration strategy requires a higher voltage (u_{cab}) compared to the initial performance (u_{ini}) with pure hydrogen as feed [24]. Moreover, this strategy leads to a certain hydrogen loss due to a fast oxidation of hydrogen with oxygen to water. Also, membrane degradation can be an issue [28].

Electrooxidation can be carried out continuously by switching the cell potential between the initial value u_{ini} and the regeneration potential u_{reg} as shown in Fig. 8, B. The regeneration potential u_{reg} must be above 0.57 V to oxidize CO to CO_2 but below 0.92 V to avoid irreversible

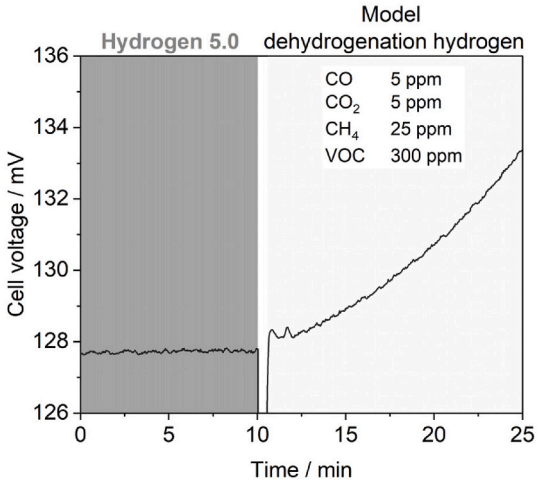

Fig. 7. Cell voltage U_{cell} over time for switching from dry hydrogen 5.0 (dark grey) to dry model hydrogen with typical impurities from the LOHC dehydrogenation (light grey). Setup: Nafion 212 membrane with a catalyst loading of 0.3 mg cm^{-2} platinum (40 % Pt/C), carbon cloth W1S1011, active membrane area of 250 cm^2, i = 0.7 A cm^{-2}, T_{cell} = 35 °C, P_{anode} =1 bar_a, $P_{cathode}$ = 3 bar_a. Humidification was achieved by circulation of liquid water on the cathode side.

platinum dissolution [29,30]. With continuous electrooxidation also hydrogen oxidation occurs, and all hydrogen is pumped out of the anode compartment. For LOHC-based hydrogen this would cause strong pressure fluctuations in the dehydrogenation reactor.

Summarizing the continuous regeneration strategies, it has to be stated that a continuous air bleeding strategy results in significant hydrogen losses, higher voltages and may lead to rapid membrane degradation while the continuous electrooxidation strategy can cause large pressure fluctuations in the dehydrogenation reactor. Due to these drawbacks, our study focused on discontinuous regeneration strategies.

Both air bleeding and electrooxidation can be implemented discontinuously by switching between pumping and regeneration mode (Fig. 8C–D). To implement discontinuous air bleeding for stable technical EHC operation, we extended the single bleeding approach from Nordio et al. [25] The discontinuous electrooxidation regeneration strategy is a new concept and is – to the best of our knowledge – investigated for the first time in this contribution. To investigate both strategies, the catalyst in the EHC is poisoned by CO during pumping mode, and the cell potential rises as a result. The regeneration mode is initiated at an arbitrary maximum potential u_{max} that is set as a compromise between increasing specific energy consumption and frequent regeneration cycles. For example, to not exceed 20 % more specific energy consumption due to linear rising voltage, the maximal potential (u_{max}) is set to 1.4 times the initial potential (u_{ini}), as a 40 %

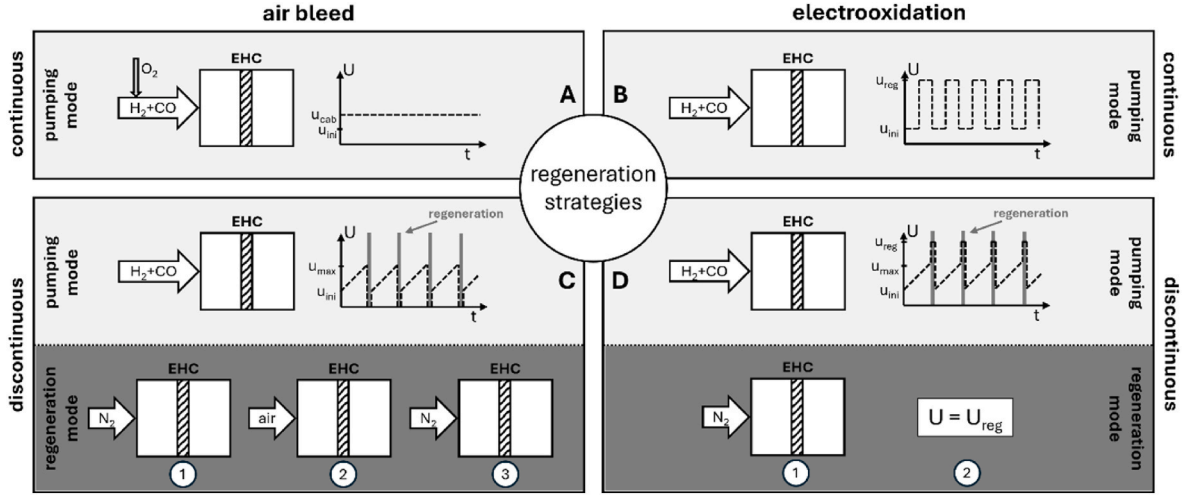

Fig. 8. Schematic representation of air bleeding and electrooxidation regeneration strategies that can be conducted continuously or discontinuously (the latter by switching between pumping and regeneration modes to counteract CO-poisoning of platinum anode catalyst).

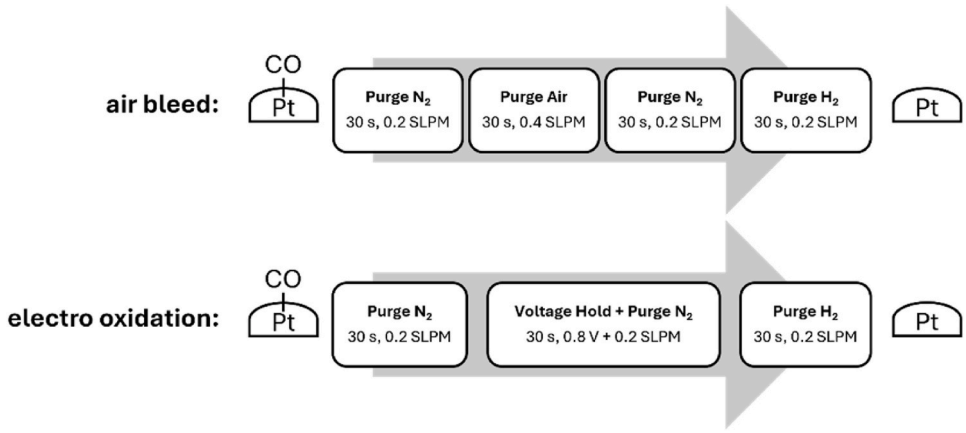

Fig. 9. Experimental parameters for discontinuous air bleeding and electrooxidation for regeneration of a CO-poisoned electrochemical hydrogen compressor. Hydrogen purge was used at the end to verify whether the initial cell voltage could be restored. This would not be required in a technical application.

increase in cell voltage results in a 20 % higher average voltage and, consequently, in 20 % more specific energy consumption.

For the discontinuous air bleed strategy (C) the following order of steps is taken during the regeneration mode: First, the anode compartment is purged with an inert gas such as nitrogen to remove hydrogen and to prevent creating an explosive atmosphere. Then, the anode compartment is purged with air to oxidize CO to CO_2. In a third step the air is purged out of the anode compartment with nitrogen for the same reason as in step one. This restores the initial cell potential.

For the discontinuous electrooxidation (D) the following steps are taken: The regeneration also starts with inertization of the anode compartment. With no hydrogen present, a subsequent voltage hold at regeneration potential u_{reg} (0.57–0.92 V) effectively electrooxidizes CO to CO_2 and restores the initial cell potential u_{ini}. During the voltage hold phase, inert gas is used to purge the anode compartment ensuring the removal of generated CO_2.

In our experiments nitrogen was used as inert gas. An additional hydrogen purge was used at the end of the regeneration to verify whether the initial cell voltage could be restored. This would not be required in a technical application. For the investigation of the parameters such as regeneration potential, volume flow of air and regeneration time, model dehydrogenation hydrogen was fed into the EHC unit. The regeneration was initiated once the cell voltage exceeded 110 % of the initial voltage. Regeneration was proven successful if the cell voltage after regeneration matched the initial cell voltage.

In general, a purge time of 30 s at a nitrogen flow rate of 0.2 SLPM was required to completely fill the periphery on the way to the anode compartment and the anode compartment itself. Thus, these conditions were used as standard. For the air-bleed regeneration an air flow of 0.2 SLPM for 30 s was not sufficient to regenerate the cell successfully. Doubling the air flow rate enabled complete regeneration. In the electrooxidation experiments, only the regeneration voltage was varied (0.6, 0.7, and 0.8 V). Each test included a 30-s nitrogen purge at 0.2 SLPM followed by holding the respective voltage for 30 s at the same flow rate. Regeneration at 0.6 V was not successful, whereas regeneration at 0.8 V proved significantly more reliable than at 0.7 V.

Both discontinuous regeneration strategies were successfully applied, following the experimental parameters shown in Fig. 9. In electrooxidation, it was necessary to ensure that the cathode compartment remained filled with hydrogen during regeneration to maintain the correct regeneration potential to SHE. For this purpose, the water flow was redirected by opening valve V_{bp1} and closing valve V_{bp2}, preventing water from displacing the hydrogen in the cathode.

Purging with 0.2 L_n min^{-1} for 30 s was necessary to completely fill the periphery on the way to the anode compartment and the anode compartment itself with the respective gas. However, the volume of the anode compartment was only 8.1 mL (see ESI sec.3). Thus, only 8.1 % of the gas was used for purging the anode compartment. In technical applications, minimizing the periphery volume could significantly reduce the required gas amount. Consequently, the regeneration time could also be significantly shortened. Due to fast regeneration and little gas consumption the discontinuous electrooxidation is the most effective regeneration strategy.

3.3. Demonstration of continuous operation

As next step, our goal was to demonstrate long-term operation of hydrogen release and compression using an EHC with discontinuous electrooxidation for regeneration. The H12-BT dehydrogenation was operated at 242 °C and atmospheric pressure. Fig. 10 shows the EHC cell voltage U_{cell} over 9 h of operation. Grey areas mark feeding of hydrogen 5.0 and white areas marks feeding of LOHC-based hydrogen from the dehydrogenation reactor. No additional filter was used in the case of LOHC-based hydrogen and only condensation at 5 °C took place before the feed entered the EHC unit. Since no additional activated carbon filter was used, 189.1 ppm VOCs and 2.7 ppm SVOCs were present in the LOHC-based hydrogen.

Interestingly, we managed to demonstrate stable operation of the EHC with LOHC-based hydrogen over more than 8 h with a total of 19 regeneration cycles. The voltage increase from before the first to after the last cycle showed was only 0.10 mV h^{-1}. The same experiment was conducted with a silica filter before the EHC and with hydrogen 5.0 for comparison. Remarkably, both experiments showed a similar voltage increase, thereby eliminating impurities such as VOCs or SVOCs as major cause for the observed minor level of degradation. By increasing the EHC cell temperature from 35 °C (as shown in Fig. 10) to 65 °C, a significantly higher voltage increase, and degradation was observed. This indicates that the membrane slightly dehydrates during operation. Since the effect of insufficient humidification is reversible, future cell designs could consider an optimized humidification concept.

A closer inspection of experimental periods in which the LOHC-based hydrogen with 41.3 ppm CO was fed into the EHC (white area in Fig. 10) shows that the cell voltage increases with CO in the hydrogen feed, as expected. When the cell voltage exceeded 57.0 mV, the electrooxidation according to Fig. 9 was initiated to regenerate the catalyst. The poisoning-induced voltage increase was arbitrarily limited to approx. 40 %, as a linear rise in cell voltage results in a 20 % higher average cell voltage – and thus limits the increase in specific energy consumption to 20 %. The experimentally determined increase in cell voltage per time of feeding hydrogen with 41.3 ppm CO-containing and active area was

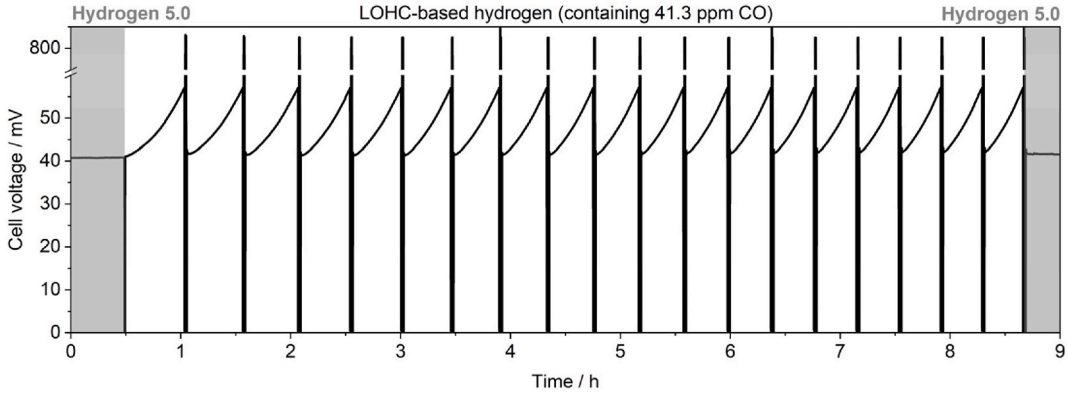

Fig. 10. Cell voltage U_{cell} over time for different feeds: hydrogen 5.0 (dark grey areas) and raw LOHC-based hydrogen containing impurities shown in Fig. 11 (white area). Discontinuous electrooxidation as regeneration strategy. Setup: Nafion 212 membrane with a catalyst loading of 0.3 mg cm^{-2} platinum (40 % Pt/C), carbon cloth W1S1011, active membrane area of 250 cm^2, i_{set} = 0.2 A cm^{-2}, T_{cell} = 35 °C, $P_{anode} = P_{cathode}$ = 1 bar_a. Humidification was achieved by circulation of liquid water on the cathode side. Setup dehydrogenation reactor: $T_{reactor}$ = 242 °C, $P_{reactor}$ = 1 bar_a, $\dot{V}_{H12-BT}$ = 3.0 mL min^{-1}, $\dot{V}_{H_2}$ = 0.39 L_n min^{-1}, conversion = 24 %, $T_{condenser}$ = 5 °C.

0.17 mV cm^{-2} h^{-1}. The regeneration time needed corresponded to 3.9 % of EHC operation time with impure LOHC-based hydrogen under the applied conditions. Furthermore, during the electrooxidative regeneration, 1.1 % of the hydrogen was lost by purging (see ESI sec.4 for details). Finally, the required energy to uphold the electrooxidation voltage would add a calculated share of 1.1 % or 2.6 % to the specific energy consumption of the EHC for the scenarios 1 or 2, respectively (see ESI sec.5 for details).

As a further scenario, we considered hydrogen release from H12-BT at a total pressure of 5 bar_a and EHC compression to 100 bar_a. Such a release and compression scenario is relevant for the filling of the medium pressure storage tank of a hydrogen filling station [16,17]. Hydrogen release from H12-BT at a pressure level of 5 bar_a has been shown to result in typical CO impurities of 2.6 ppm [7,15]. In this case, regeneration by electrooxidation would only require 0.2 % of the time of hydrogen compression. During such short regeneration phases, a slight pressure increase in the dehydrogenation reactor would be expected (due to continued hydrogen production without exit to the EHC), but no hydrogen would be lost. Regeneration intervals would be realized approximately every 6 h if the same voltage increase of $u_{max} = 1.4 \bullet u_{ini}$ is allowed. Thus, purging losses would be reduced to 0.07 %. Also, the additionally required specific energy consumption for electrooxidation would be reduce to 0.31 %. For the EHC operation the compression ratio is 20 as for Scenario 1. Due to the same compression ratio, the Nernst voltage remains the same. However, the current efficiency decreases from 95.3 to 76.6 % because of the higher pressure difference compared to Scenario 1. Thus, the specific energy consumption would increase from 2.00 (compression from 1 to 20 bar_a) to 2.97 kWh_{el} $kg^{-1}_{hydrogen}$ (compression from 5 to 100 bar_a) for EHC operation with impure hydrogen using a N212 membrane at 35 °C cell temperature and a current density of 0.2 A cm^{-2} including regeneration by electrooxidation.

3.4. Hydrogen output quality

To determine the hydrogen purity at the EHC output when operating with LOHC-based hydrogen we used an analytical FTIR device calibrated for measuring typical impurities in hydrogen in the ppm range [5,7,34]. Fig. 11 shows the measured impurities in the product hydrogen before and after passing through the EHC. For comparison, measurements with hydrogen 5.0 from the gas supply of our laboratory is also shown. In the LOHC-based hydrogen feed to the EHC, higher CO and CO_2 concentrations and lower CH_4 concentrations are found compared to values published by Zilm et al. [7] This difference is due to the lower reaction temperature and pressure in our experiments compared to Zilm et al. and, consequently a lower tendency to convert CO and CO_2 into methane by methanation. The VOC concentration was in the range of the values published by Zilm et al. (for details on SVOCs see ESI sec.6).

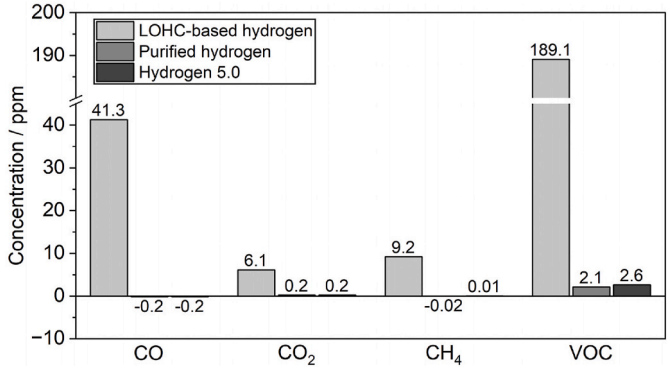

Fig. 11. Impurities in LOHC-based hydrogen (light grey), purified hydrogen (grey) and hydrogen 5.0 (dark grey) measured with an FTIR. Setup EHC: Nafion 212 membrane with a catalyst loading of 0.3 mg cm^{-2} platinum (40 % Pt/C), carbon cloth W1S1011, active membrane area of 250 cm^2, i_{set} = 0.2 A cm^{-2}, T_{cell} = 35 °C, $P_{anode} = P_{cathode}$ = 1 bar_a. Humidification was achieved by circulation of liquid water on the cathode side. Setup dehydrogenation reactor: $T_{reactor}$ = 242 °C, $P_{reactor}$ = 1 bar_a, $\dot{V}_{H12-BT}$ = 3.0 mL min^{-1}, $\dot{V}_{H_2}$ = 0.39 Ln min^{-1}, conversion = 24 %, $T_{condenser}$ = 5 °C.

A comparison of the measured concentrations in purified hydrogen and hydrogen 5.0 shows that the concentrations in purified hydrogen are equal to or even lower than those in hydrogen 5.0. This indicates that all measured impurities were successfully removed. Note that we cannot directly measure SVOCs with our FTIR analysis. However, the assumption of their absence is supported by two arguments. First, since no VOCs were detected on the cathode side and diffusion is the only mechanism by which impurities can reach this side, we assume that SVOCs are also absent in the produced hydrogen. This assumption is justified, as according to Fick's law and assuming Knudsen diffusion, SVOCs would diffuse much more slowly (by about two orders of magnitude) through the membrane than VOCs due to their larger molecular diameter and lower concentration. Second, Zilm et al. reported a cross-sensitivity of their FTIR to VOCs and SVOCs when comparing GC and FTIR data, with minor SVOC traces appearing in the FTIR signal due to this cross-sensitivity [7]. Thus, if SVOCs had crossed the membrane, a corresponding signal would have been expected in the FTIR spectrum. Since no VOC-related signal was observed, the presence of SVOCs can therefore be excluded.

The purified hydrogen is fully saturated with water at the cell temperature due to the cathode-side humidification of the cell with liquid water. Apart from this, purification to ISO norm 14687-2 standard is possible with the LOHC dehydrogenation + EHC setup applied in this study. While for application of the released hydrogen in a filling station, the removal of water is necessary (due to the hydrogen cooling in the high pressure stage of the filling station), the humidity may even be an advantage if the hydrogen is directly used in a fuel cell. To provide ISO-compliant hydrogen, a drying step must be considered in the overall energetic analysis. For the compression of LOHC-based hydrogen from 5 to 100 bar_a using EHC technology, the specific energy consumption for condensation-based drying was calculated to 0.25 kWh_{el} $kg^{-1}_{hydrogen}$, as shown in Section 6 of the ESI. Including this drying step, the total specific energy consumption amounts to 3.22 kWh_{el} $kg^{-1}_{hydrogen}$.

The data from the results section of this publication are also available via Zenodo [35].

4. Conclusion

This study investigates the continuous supply of purified and compressed hydrogen from a Liquid Organic Hydrogen Carrier (LOHC) dehydrogenation process while aiming for minimal specific energy consumption. An electrochemical hydrogen compressor (EHC) has been used downstream to the dehydrogenation reactor to meet this goal. The EHC was humidified using only a liquid water circulation through the cathode compartment, while the supplied hydrogen was not additionally humidified. An energetic evaluation was conducted to optimize the EHC membrane selection. Membranes were tested at temperatures ranging from 35 to 65 °C, with a focus on Nafion 212, 115 and 117. Key parameters were evaluated such as the Nernst voltage which was calculated by considering the vapor pressure of water on both sides. The cell voltage was measured in form of polarization curves and the permeability coefficients were determined to calculate current efficiencies. The performance of the applied EHC setup was assessed based on cell temperature, membrane thickness, and compression ratio. Among the evaluated membranes, the N212 membrane exhibited the lowest specific energy consumption in different compression scenarios in a current density range of 0.1–0.8 A cm^{-2}. The specific energy consumption was between 1.65 and 4.15 kWh $kg^{-1}_{hydrogen}$ for a compression ratio of 20 and between 2.84 and 4.97 kWh $kg^{-1}_{hydrogen}$ for a compression ratio of 70. These values refer exclusively to the electrical energy demand for electrochemical compression. The efficiency of the LOHC

dehydrogenation is not considered, as it strongly depends on the applied heat integration concept [31].

To address the issue of EHC catalyst poisoning by CO from the LOHC-based hydrogen, our study explored different regeneration strategies. Continuous and discontinuous air bleeding and electrooxidation were evaluated. Discontinuous methods proved to be favourable due to lower hydrogen losses, reduced membrane degradation and less fluctuating pressure in the dehydrogenation reactor. Discontinuous electrooxidation was particularly effective, offering fast regeneration with low gas consumption. The optimal regeneration process involved purging with inert gas for 60 s and maintaining a voltage of 0.8 V to regenerate the catalyst. Implementing the discontinuous electrooxidation into an EHC operation with LOHC-based hydrogen containing a CO content of 2.6 ppm, a typical start pressure from dehydrogenation of 5 bar_a and a target pressure after compression to 100 bar_a (scenario of filling a medium pressure storage tank at a hydrogen filling station) led to a specific energy consumption of 3.22 kWh_{el} $kg^{-1}_{hydrogen}$ for the N212 membrane (cell temperature = 35 °C; current density of 0.2 A cm^{-2}, including condensation-based drying step). The calculated hydrogen losses due to purging are 0.07 % in this case.

The practical application of these findings was demonstrated through 8-h continuous operation of the EHC as single downstream unit for the LOHC-based hydrogen, which included 19 regeneration cycles using electrooxidation. During this extended operation, the system maintained stability and effective hydrogen compression and cleaning. The raw hydrogen from the LOHC release unit containing 41.3 ppm CO and 2.7 ppm SVOCs was successfully purified to meet ISO standards on a wet basis. Overall, these findings highlight the potential for efficient hydrogen purification and compression with an EHC in combination with LOHC-based hydrogen storage technologies.

In future work, pilot-scale operation at a higher outlet pressure should be investigated to validate the findings under industrially relevant conditions and to demonstrate long-term operational stability over extended periods. Moreover, optimization of the cell design, especially regarding humidification with liquid water on the cathode side, as well as a systematic parametric study of the discontinuous electrooxidation (d-EO) regeneration protocol, are expected to further improve system efficiency. A key future challenge is to identify a membrane thickness that simultaneously ensures sufficient proton conductivity and mechanical stability under elevated pressure differentials. Furthermore, membrane stability needs to be validated for a high differential pressure over an industrially relevant time on stream. Additional performance improvements may also be achieved through chemical or structural membrane modifications.

CRediT authorship contribution statement

M. Blasius: Writing – original draft, Visualization, Investigation, Formal analysis, Data curation, Conceptualization. **S. Pappler:** Writing – review & editing, Validation, Investigation. **T. Mader:** Writing – review & editing, Validation, Investigation. **S. Mrusek:** Writing – review & editing, Methodology, Conceptualization. **T. Rüde:** Writing – review & editing, Supervision, Methodology, Conceptualization. **M. Geißelbrecht:** Writing – review & editing, Supervision, Resources, Project administration, Methodology, Conceptualization. **P. Wasserscheid:** Writing – review & editing, Supervision, Resources, Project administration, Methodology, Funding acquisition, Conceptualization.

Declaration of competing interest

Peter Wasserscheid is founder and minority share holder of the company Hydrogenious LOHC Technologies (www.hydrogenious.net) that offers commercially hydrogen storage systems based on the LOHC technology.

There is no conflict of interest to declare with regard to the specific scientific results reported in this paper.

Acknowledgement

The authors acknowledge financial support by the Bavarian Ministry of Economic Affairs, Regional Development and Energy through the project “Wasserstoff —Abscheidung aus dem Erdgas-Verteilnetz” (84-6665a2/162/01). Additionally, the authors like to thank Axel Marth, Dominik Venus and Maximilian Maier for helpful discussions.

Appendix A. Supplementary data

Supplementary data to this article can be found online at https://doi.org/10.1016/j.ijhydene.2025.153039.

References

[1] Distel MM, Margutti JM, Obermeier J, Nuß A, Baumeister I, Hritsyshyna M, Weiß A, Neubert M. Large-scale H2 storage and transport with liquid organic hydrogen carrier technology: insights into current project developments and the future outlook. Energy Technol 2024:2301042.
[2] Rhandi M, Trégaro M, Druart F, Deseure J, Chatenet M. Electrochemical hydrogen compression and purification versus competing technologies: part I. Pros and cons. Chin J Catal 2020;41(5):756–69.
[3] Bouwman P. Electrochemical hydrogen compression (EHC) solutions for hydrogen infrastructure. Fuel Cell Bull 2014;2014(5):12–6.
[4] Sdanghi G, Maranzana G, Celzard A, Fierro V. Review of the current technologies and performances of hydrogen compression for stationary and automotive applications. Renew Sustain Energy Rev 2019;102:150–70.
[5] Mrusek S, Preuster P, Müller K, Bösmann A, Wasserscheid P. Pressurized hydrogen from charged liquid organic hydrogen carrier systems by electrochemical hydrogen compression. Int J Hydrogen Energy 2021;46(29):15624–34.
[6] Mrusek S, Blasius M, Morgenroth F, Thiele S, Wasserscheid P. Hydrogen extraction from methane-hydrogen mixtures from the natural gas grid by means of electrochemical hydrogen separation and compression. Int J Hydrogen Energy 2024;50:526–38.
[7] Zilm A, Ortner F, Gackstatter F, Koeberlein S, Kadar J, Geisselbrecht M, Boesmann A, Wasserscheid P. Impurities in hydrogen released from perhydro benzyltoluene-assessment and adsorptive removal. Int J Hydrogen Energy 2025;101:469–81.
[8] Marciuš D, Kovač A, Firak M. Electrochemical hydrogen compressor: recent progress and challenges. Int J Hydrogen Energy 2022;47(57):24179–93.
[9] HyET. Productsheet (the new standard in hydrogen compression): https://hyethydrogen.com/upload_directory/files/BI1207-hydrogen-flyer-2020.001.04.pdf. [cited 2025/10/18.].
[10] Rüde T, Dürr S, Preuster P, Wolf M, Wasserscheid P. Benzyltoluene/perhydro benzyltoluene–pushing the performance limits of pure hydrocarbon liquid organic hydrogen carrier (LOHC) systems. Sustain Energy Fuels 2022;6(6):1541–53.
[11] Kwak Y, Kirk J, Moon S, Ohm T, Lee Y-J, Jang M, Park L-H, Ahn C-i, Jeong H, Sohn H. Hydrogen production from homocyclic liquid organic hydrogen carriers (LOHCs): benchmarking studies and energy-economic analyses. Energy Convers Manag 2021;239:114124.
[12] Müller K, Stark K, Emel’yanenko VN, Varfolomeev MA, Zaitsau DH, Shoifet E, Schick C, Verevkin SP, Arlt W. Liquid organic hydrogen carriers: thermophysical and thermochemical studies of benzyl-and dibenzyl-toluene derivatives. Ind Eng Chem Res 2015;54(32):7967–76.
[13] Brückner N, Obesser K, Bösmann A, Teichmann D, Arlt W, Dungs J, Wasserscheid P. Evaluation of industrially applied heat-transfer fluids as liquid organic hydrogen carrier systems. ChemSusChem 2014;7(1):229–35.
[14] Preuster P, Papp C, Wasserscheid P. Liquid organic hydrogen carriers (LOHCs): toward a hydrogen-free hydrogen economy. Acc Chem Res 2017;50(1):74–85.
[15] Willer M, Preuster P, Geißelbrecht M, Wasserscheid P. Continuous dehydrogenation of perhydro benzyltoluene and perhydro dibenzyltoluene in a packed bed vertical tubular reactor–the role of LOHC evaporation. Int J Hydrogen Energy 2024;57:1513–23.
[16] Apostolou D, Xydis G. A literature review on hydrogen refuelling stations and infrastructure. Current status and future prospects. Renew Sustain Energy Rev 2019;113:109292.
[17] Farzaneh-Gord M, Deymi-Dashtebayaz M, Rahbari HR, Niazmand H. Effects of storage types and conditions on compressed hydrogen fuelling stations performance. Int J Hydrogen Energy 2012;37(4):3500–9.
[18] standardization Iof. ISO/DIS 14687 Hydrogen fuel quality–Product specification. Geneva, Switzerland: International Organisation for Standardization; 2019.
[19] Verevkin SP, Vostrikov SV, Leinweber A, Wasserscheid P, Müller K. Thermochemical properties of benzyltoluenes and their hydro-and perhydro-derivatives as key components of a liquid organic hydrogen carrier system. Fuel 2023;335:126618.
[20] Baschuk J, Li X. Carbon monoxide poisoning of proton exchange membrane fuel cells. Int J Energy Res 2001;25(8):695–713.
[21] Reshetenko TV, Bethune K, Rubio MA, Rocheleau R. Study of low concentration CO poisoning of Pt anode in a proton exchange membrane fuel cell using spatial electrochemical impedance spectroscopy. J Power Sources 2014;269:344–62.
[22] Ree J, Kim Y, Shin H. Reaction of atomic oxygen with adsorbed carbon monoxide on a platinum surface. J Chem Phys 1996;104(2):742–57.

[23] Mananghaya MR. Adsorption of CO and desorption of CO2 interacting with Pt (111) surface: a combined density functional theory and Kinetic Monte Carlo simulation. Adsorption 2020;26(3):461–9.
[24] Jackson C, Raymakers L, Mulder M, Kucernak A. Poison mitigation strategies for the use of impure hydrogen in electrochemical hydrogen pumps and fuel cells. J Power Sources 2020;472:228476.
[25] Nordio M, Barain ME, Raymakers L, Annaland MVS, Mulder M, Gallucci F. Effect of CO2 on the performance of an electrochemical hydrogen compressor. Chem Eng J 2020;392:123647.
[26] Gardner C, Ternan M. Electrochemical separation of hydrogen from reformate using PEM fuel cell technology. J Power Sources 2007;171(2):835–41.
[27] Dey S, Dhal G. Property and structure of various platinum catalysts for low-temperature carbon monoxide oxidations. Mater Today Chem 2020;16:100228.
[28] Inaba M, Kinumoto T, Kiriake M, Umebayashi R, Tasaka A, Ogumi Z. Gas crossover and membrane degradation in polymer electrolyte fuel cells. Electrochim Acta 2006;51(26):5746–53.
[29] Anderson AB, Neshev NM. Mechanism for the electro-oxidation of carbon monoxide on platinum, including electrode potential dependence: theoretical determination. J Electrochem Soc 2002;149(10):E383.
[30] Cherevko S, Kulyk N, Mayrhofer KJ. Durability of platinum-based fuel cell electrocatalysts: dissolution of bulk and nanoscale platinum. Nano Energy 2016;29:275–98.
[31] Müller K, Thiele S, Wasserscheid P. Evaluations of concepts for the integration of fuel cells in liquid organic hydrogen carrier systems. Energy Fuels 2019;33(10):10324–30.
[32] Kim C, Gong M, Lee J, Na Y. Minimizing specific energy consumption of electrochemical hydrogen compressor at various operating conditions using Pseudo-2D model simulation. Membranes 2022;12(12):1214.
[33] Schalenbach M, Hoefner T, Paciok P, Carmo M, Lueke W, Stolten D. Gas permeation through nafion. Part 1: measurements. J Phys Chem C 2015;119(45):25145–55.
[34] Bulgarin A, Jorschick H, Preuster P, Bösmann A, Wasserscheid P. Purity of hydrogen released from the liquid organic hydrogen carrier compound perhydro dibenzyltoluene by catalytic dehydrogenation. Int J Hydrogen Energy 2020;45(1):712–20.
[35] Blasius M, Pappler S, Mader T, Schärfe T, Geißelbrecht M, Wasserscheid P. Dataset for publication: upgrading LOHC-based hydrogen through electrochemical hydrogen compression for fuel cell applications. Zenodo; 2025.